Vol. 08, No. 3 (2026) 1653-1672, doi: 10.24874/PES08.03.020

Proceedings on Engineering Sciences

www.pesjournal.net

PREDICTING TRIBOLOGICAL PERFORMANCE OF GRAPHITE-PLUGGED BRONZE BUSHINGS USING AN ADAPTIVE NEURO-FUZZY INFERENCE SYSTEM

Ali K. A. Aljboury[1]
Amir Alsammarraie
Maki H. Zaidan

Received 03.06.2026
Revised 10.07.2026
Accepted 18.08.2026

Keywords:

ANFIS, Graphite-plugged bronze bushings, Coefficient of friction, Material loss, Tribological prediction, Self-lubricating bearings

A B S T R A C T

Graphite-plugged bronze bushings are widely used in industrial applications where conventional lubrication is not feasible, yet predicting their tribological behavior remains difficult due to the nonlinear interactions among material composition, plug geometry, and operating conditions. This paper presents two independent ANFIS models—one for coefficient of friction (COF) and one for material loss—developed and validated against dry sliding experimental data from CuAl10Fe5Ni5 bushings running against an AISI 410 stainless steel shaft. The training dataset came from 81 full-factorial tests across four input variables: graphite surface coverage (10, 20, 30%), plug diameter (8, 10, 12 mm), rotational speed (250, 500, 750 rpm), and applied load (50, 100, 150 kg). Each model uses a zero-order Takagi-Sugeno-Kang fuzzy structure with triangular membership functions on a 3×3×3×3 grid, producing 81 IF-THEN rules, trained over 200 epochs with a hybrid least-squares/backpropagation algorithm. MATLAB ANFIS training converged to final RMSE values of 0.00097889 for COF and 0.00636561 g for material loss. Validation against three previously unseen operating conditions produced maximum prediction errors of 1.20% and 3.927%, respectively—indicating satisfactory interpolation accuracy within the investigated parameter range. The results suggest that ANFIS can accurately predict the nonlinear tribological behavior of graphite-plugged bronze bushings and can reduce the extent of physical testing required during preliminary design evaluation across the interpolated operating range.

© 2026 Published by Faculty of Engineering

1. INTRODUCTION

Graphite-plugged bronze bushings—also called oilless or self-lubricating bearings—are standard in heavy-duty industrial applications such as pumps, hydraulic machinery, mining equipment, and marine drives, where oil lubrication is impractical. The design pairs the mechanical strength and wear resistance of the bronze matrix with the low-shear, layered-lattice structure of embedded graphite. During operation, graphite transfers gradually from the plugs to the contact surfaces, forming a thin carbon film that reduces friction and extends service life. Research on Cu-graphite and bronze-based self-lubricating composites has shown that graphite content directly governs the graphite-rich friction/transfer film: at optimized levels, a stable tribolayer forms on worn surfaces and sustains

[1] Corresponding author: Ali K. A. Aljboury
Email: eng.alikhalaf1982@gmail.com

low-friction sliding (Güngör & Demirer, 2022; Zhu, Yi, Ge, Zhang, & Xie, 2022).

Tribological performance—measured by COF and material loss—depends on the interaction among graphite content, plug geometry, sliding speed, and applied load. Sliding speed is particularly damaging: material loss can increase by over 300% as speed rises from 250 to 750 rpm, driven largely by thermal degradation of the graphite film (Alsammarraie, Zaidan, & Aljboury, 2026). These interactions matter for bearing design, but their nonlinearity makes conventional analytical and empirical models unreliable, leading to challenges in accurately predicting performance under varying conditions. Full experimental characterization across the complete parameter space is accurate but time-consuming and resource-intensive.

Machine learning methods have been applied in tribology to build predictive surrogate models from experimental data. For copper/aluminum-graphite self-lubricating composites, algorithms including support vector machines, random forests, and gradient boosting have correlated friction and wear rates with material composition, lubricant content, and test conditions—handling multivariate complexity that analytical approaches cannot. ANNs have performed well for nonlinear input-output mapping in friction and wear prediction across bearing materials, polymer composites, and coatings. Ünlü et al. applied an ANN to journal bearings under dry and lubricated conditions, showing the model could reduce reliance on physical testing (Ünlü, Durmuş, & Meriç, 2012). Milčić et al. (2021) developed two separate 3-6-1 backpropagation ANN models for tin-babbitt journal bearings, reaching mean absolute percentage errors of 0.0054% and 0.0085% for friction coefficient training and testing, respectively (Milčić, Alsammarraie, Madić, Krstić, & Milčić, 2021). What ANNs do not provide is any window into the relationships they learn—they are accurate but opaque.

ANFIS, introduced by Jang in 1993, was built to solve exactly that problem. It embeds a Takagi-Sugeno-Kang fuzzy inference system within a five-layer adaptive network trained by a hybrid algorithm, pairing the learning power of neural networks with the transparent IF-THEN rule structure of fuzzy logic. A study comparing ANN, ANFIS, and fuzzy clustering for wear prediction in sintered steel found that all three outperformed conventional models, with ANFIS producing the best trade-off between predictive accuracy and rule transparency (Alambeigi, Khadem, Khorsand, & Mirza Seied Hasan, 2016). Training uses least-squares estimation in the forward pass and gradient-descent backpropagation in the backward pass—a faster convergence and more reliable parameter identification than pure gradient descent. A zero-order TSK structure with triangular membership functions keeps the rule base compact without sacrificing fit. Recent work by Marhoon and Al-Sammarraie suggested that ANFIS accurately predicts friction coefficient and material loss in copper-based alloys under variable loads, achieving prediction errors as low as 0.67% for COF — further confirming the method's suitability for tribological modeling of bearing materials (Marhoon & Al-Sammarraie, 2025).

Its application to graphite-plugged bronze bushings under dry sliding, however, has not been reported. Recent tribology work has moved toward ensemble frameworks that predict multiple outputs simultaneously (Kumbhar, Gadade, Singh, & Choudhary, 2026), but these give up the interpretability that the fuzzy rule base provides. Studies in this area focus on polymer-matrix composites, lubricated metallic systems, or single-output models(Alambeigi et al., 2016; Ning et al., 2024). Predicting COF and material loss together as functions of four material and operating parameters in CuAl10Fe5Ni5 bronze-graphite bushings is the gap this work addresses.

The experimental training data set in this study is selected from a larger factorial investigation of tribological behavior of graphite-plugged CuAl10Fe5Ni5 bronze bushings published by Alsammarraie et al. (Alsammarraie et al., 2026). In that study, tribological performance was characterized under 81 operating conditions at three different sliding time intervals (10, 20 and 30 minutes) and in the present paper, the 30-minute subset was used as the training data for the ANFIS, representing the longest sliding duration tested and the closest approach to a stable tribological state within the tested time window (see Section 2.4 for a discussion of running-in versus steady-state behavior). It is distinguished in three aspects: (1) Two independent ANFIS predictive models for COF and material loss are developed, trained, and validated. (2) Three independent experiments with operating conditions different from the 81-point training set are conducted for both validation, and (3) 3D response surfaces are generated and analyzed for their main input parameters and interactions. No experimental data were changed from what was reported in (Alsammarraie et al., 2026).

2. MATERIALS AND EXPERIMENTAL PROCEDURES

2.1 Bushing Material and Geometry

Test bushings were obtained from Jiashan PVB Sliding Bearing Co., Ltd., China, and manufactured from CuAl10Fe5Ni5 nickel-aluminum bronze. This alloy is the standard choice for graphite-plugged oilless bushings, selected for its wear resistance, corrosion protection, and load-carrying capacity. Chemical composition and mechanical properties were verified and certified by Zhejiang Haima Transmission Technology Co., Ltd.; both are reported in Tables 1 and 2 alongside the applicable standard ranges. All batch values conform to specification.

Table 1. Chemical composition (wt%) of CuAl10Fe5Ni5 bronze alloy

Element	Cu	Al	Fe	Ni	Mn	Zn	Pb	Sn	Si
Standard range	76–83	8–11	4.0–6.0	4.0–6.0	0.5–2.5	≤0.5	≤0.1	≤0.2	≤0.3
Batch average	79.88	9.22	5.14	4.76	0.99	0.01	0	0	0

Table 1. Mechanical properties of CuAl10Fe5Ni5 bronze alloy

Property	Yield strength (MPa)	Tensile strength (MPa)	Elongation (%)	Hardness (HB)
Standard	≥200	≥590	≥6	170–260
Average	233	618	8	207

Graphite plugs of high-purity carbon (≥99.5%, density 1.56 g/cm³) were pressed into pre-drilled recesses in the bronze matrix under high pressure. All bushings shared the same external dimensions: 40 mm inner diameter × 50 mm outer diameter × 40 mm length. Three plug diameters were tested — 8, 10, and 12 mm — at three levels of graphite surface coverage: 10%, 20%, and 30% of the inner bore area.

2.2 Counterface Shaft

The rotating shaft was machined from AISI 410 martensitic stainless steel sourced from the Northern Refineries Company, Iraq. This grade was chosen for its hardness and wear resistance, properties typical of shaft materials in petroleum refining and pump service. Before each test, the shaft surface was hand-polished with 1000-grit emery paper to restore a consistent counterface condition. Roughness was measured at five locations; the average was Ra = 0.474 µm. Composition and hardness are reported in Table 3.

Table 2. Chemical composition and hardness of AISI 410 stainless steel shaft

C	Mn	Si	P	S	Cr	Ni	Fe	Hardness (HB)
0.12	0.9	0.8	0.03	0.02	12.5	0.68	balance	243

2.3 Experimental Setup

A custom journal-bearing tribometer (Figure 1) was designed in SolidWorks and manufactured locally at Tikrit University to replicate actual journal bearing geometry and loading conditions. The rig is driven by an AC motor connected to a steel shaft, which runs inside a housing assembly fabricated from 10 mm carbon steel plate with upper and lower jaws. Normal force is measured by an S-beam load cell (SS300, 200 kg capacity), and friction force is acquired through a bending-beam load cell (OIML R60 C3-class, 25 kg capacity). Shaft speed is regulated by a Delta VFD-EL variable frequency drive, capable of speeds up to 3000 rpm. Contact temperature at the bushing–shaft interface is monitored by a K-type thermocouple connected to a CH102 digital temperature controller with a measurement range of 0–400°C.

The diametral clearance between the bushing bore and shaft was held at 0.02 mm across all specimens. Bushing mass was recorded before and after each test on a Sartorius BL210S analytical balance (0.1 mg readability, 210 g capacity) to determine material loss. Surface roughness was measured with an LS310 contact profilometer (Shenzhen Qifa Trade, China), stylus tip radius of a few micrometers, and Ra accuracy of 0.005 µm.

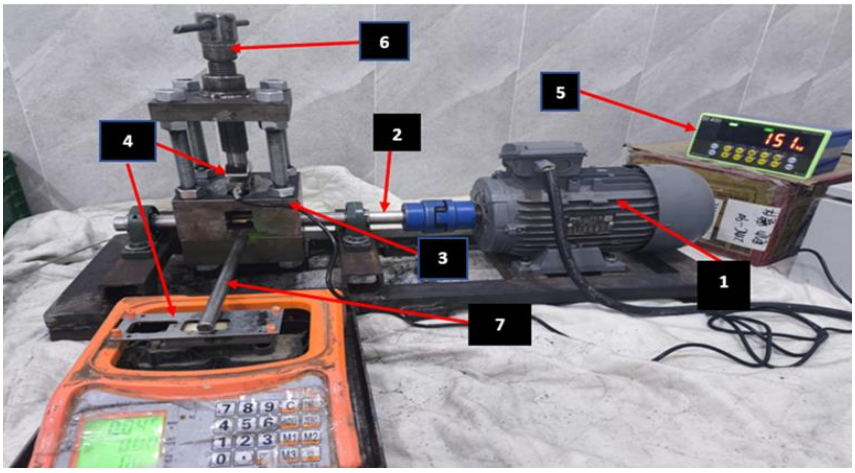


Figure 1. Experimental test rig: (1) AC motor, (2) shaft, (3) housing, (4) load cell, (5) digital indicator, (6) load transducer arm, (7) friction transducer arm

2.4 Experimental Design and Procedure

A full factorial design with four factors at three levels each (3^4) produced 81 unique test conditions per output variable, matching the 81-rule ANFIS structure described in Section 3. The factors and levels are listed in Table 4. Sliding time was fixed at 30 minutes per test, with the resulting sliding distance varying between 942 m and 2826 m depending on the rotational speed and bushing radius.

Table 3. Full-factorial experimental design parameters

Parameter	Level 1	Level 2	Level 3
A: Graphite percentage (%)	10	20	30
B: Graphite plug diameter (mm)	8	10	12
C: Sliding speed (rpm)	250	500	750
D: Applied load (kg)	50	100	150

Before each test, bushings and shaft were wiped with acetone, dried with a lint-free tissue, then held in a drying oven at 60°C for one hour to remove moisture and residual contamination. Pre-test bushing mass and inner surface roughness were recorded. The shaft was polished with 1000-grit emery paper before each run to restore the counterface to Ra = 0.474 µm.

All tests ran at ambient temperature (25°C) under dry sliding conditions, with a fixed bushing-to-shaft radial clearance of 0.02 mm. Normal load was applied through the load transducer arm before the motor started. After each test, the bushing was wiped clean, post-test mass and roughness were recorded, and material loss was calculated as the difference between pre- and post-test mass.

The experiments were carried out in accordance with the procedures of the GUM for uncertainty estimation (JCGM 100:2008). The test matrix was large, with 81 test conditions, as is common practice in conducting full factorial tribological tests. Selected representative conditions were, however, repeated to ensure repeatability.

Before each test series, the force measurement systems were calibrated with certified test weights. The S-beam load cell (SS300, 200 kg load) was calibrated using a known weight placed on the load arm of the load cell and the bending beam load cell (OIML R60 C3-class, 25 kg capacity) was calibrated by applying a known friction force to the load arm. The calibration procedures were carried out in accordance with the manufacturer's instructions and the SI400 calibration modes (test weight calibration mode and simulation calibration mode).

Shaft alignment was checked by ensuring the same diametral clearance of 0.02 mm between the bushing bore and shaft was kept constant. The housing is precisely machined to allow the shaft and bushing to be coaxial. The pre-test shaft runout was used to help control runout, and the VFD speed control was adjusted as necessary.

All friction readings were taken continuously throughout each test and recorded every 2 minutes. These reported COF values are time-averaged, rather than instantaneous. This averaging out smooths out the effects of transients and gives a more representative measure of the steady-state friction.

The recorded friction traces generally showed a plateauing trend after about 10-15 minutes of sliding (around 60-70% of the test duration). It should be noted, however, that the companion factorial study using this same dataset (Alsammarraie et al., 2026) characterized the tribological response over the same 10, 20, and 30-minute intervals as running-in behavior rather than as having reached a confirmed steady-state equilibrium. The plateauing observed in the present COF-time curves is consistent with the friction coefficient approaching a comparatively stable level within the 30-minute test window but does not by itself establish that a true steady state (as opposed to a late stage of running-in) had been reached; the two interpretations are not necessarily in conflict, since running-in can itself produce a gradually flattening COF-time curve before full equilibrium is achieved.

The expanded uncertainties (k=2, 95% confidence) for the measurement systems were calculated during the design stage, based on the GUM framework, as shown in Table 5.

Table 5. Expanded uncertainties (k=2, 95% confidence) for the measurement systems determined at the design stage using the GUM framework (JCGM 100:2008)

Measurement System	Expanded Uncertainty	Relative Uncertainty
Normal Force (SS300, 200 kg capacity)	±0.11 kg	0.055% FS
Friction Force (OIML R60 C3-class, 25 kg capacity)	±0.0202 kg	0.080% FS
Temperature (K-type thermocouple)	±3.9°C	~2.6%
Mass Loss (Sartorius BL210S)	±0.054 mg	0.54% (for 10 mg wear)
Surface Roughness (LS310)	±0.058 µm	~12%

The speed control system consisted of a Delta VFD-EL variable frequency drive and a 3-phase induction motor. The VFD frequency control was used to set the target rotational speed for each test. The actual shaft rotational speed was not independently measured or verified during the experiments (e.g., by a tachometer, optical/magnetic encoder, or stroboscope); the reported speed values (250, 500, 750 rpm, and the intermediate validation speeds) correspond to the VFD frequency setting only. Accordingly, the uncertainty reported here is the uncertainty of the VFD frequency setting itself, not a measured uncertainty of the actual shaft speed, and any additional deviation between the commanded VFD frequency and the true shaft speed (e.g., due to induction-motor slip under load) is not captured by this estimate. The speed uncertainty was estimated at the design stage using the GUM framework: the dominant contribution is the rated accuracy of the VFD output frequency (±0.5% of the maximum frequency, corresponding to ±108 rpm at all speed settings), which is the manufacturer's worst-case specification rather than a value confirmed by independent speed measurement during testing. Future work should incorporate direct shaft-speed measurement to confirm that the commanded and actual speeds coincide within this stated tolerance.

The coefficient of friction was calculated from the moment balance of the friction transducer arm as shown in Figure 2:

$$\mu = \frac{F_L}{F_N} \times \frac{L}{r} \quad (1)$$

where F_L is the measured friction force (N), F_N is the applied normal load (N), L is the distance from the load cell attachment point to the shaft centre (mm), and r is the bushing inner radius (mm).

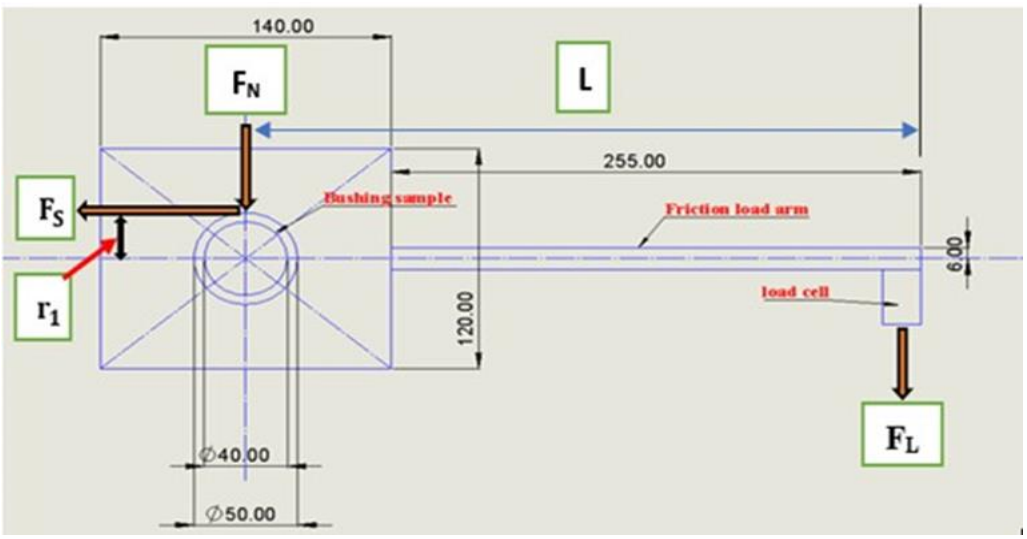


Figure 2. Schematic of the friction force measurement mechanism

3. ANFIS METHODOLOGY

3.1 Theoretical Background

ANFIS, introduced by Jang (1993), is a five-layer feedforward adaptive network that implements a Takagi-Sugeno-Kang (TSK) fuzzy inference system (Jang, 1993). It combines the learning and computational capability of neural networks with the transparent IF-THEN rule structure of fuzzy logic (Walia, 2015). Both the membership function parameters (premise parameters) and the rule consequent parameters are tuned automatically from training data, removing the need for manually derived expert rules (Karaboga & Kaya, 2019).

Neuro-fuzzy systems can be understood simultaneously as adaptive fuzzy inference systems that learn rules from data and as connectionist architectures with linguistic meaning attached to their structure (Vesović & Jovanović, 2022). In tribological modeling, this approach is a practical advantage: physical insight can be encoded in the rule structure while the hybrid learning algorithm refines the quantitative parameters from experimental measurements (Salim, Saini, Matharu, & Singh, 2023).

3.1 ANFIS Architecture

For the four-input, single-output configuration used here, ANFIS implements a zero-order TSK model in which each rule's consequent is a constant (singleton) (Jang, 1993). Each input variable is partitioned into three triangular membership functions, producing $3^4 = 81$ IF-THEN rules (Talpur, Salleh, & Hussain, 2017). The five-layer architecture operates as follows: Layer 1 (Fuzzification) computes membership grades using triangular functions; Layer 2 (Rule Strength) computes firing strengths as the product of incoming membership grades. Layer 3 (Normalization) normalizes firing strengths across all 81 rules. Layer 4 (Consequent) computes weighted rule outputs using singleton constants identified by least-squares estimation. Layer 5 (Output) sums all weighted outputs into the final crisp prediction (Jang, 1993).

3.2 ANFIS Model Construction Procedure

Two independent ANFIS models were built in MATLAB's Fuzzy Logic Toolbox—one for COF and one for material loss. Both share the same construction procedure, carried out in the following steps.

Step 1 — Input and output definition. Four input variables were defined: graphite surface coverage percentage (%), plug diameter (mm), rotational speed (rpm), and applied load (kg). The output variable was defined separately for each model: COF (dimensionless) and material loss (g).

Step 2 — Membership function assignment. Each input was partitioned into three triangular membership functions (trimf) using grid partitioning, producing a 3×3×3×3 input space with 81 rules. Parameters were initialized uniformly across each input range and tuned during training (Talpur et al., 2017). The COF and material loss ANFIS network structures are shown in Figures 3 and 4, respectively.

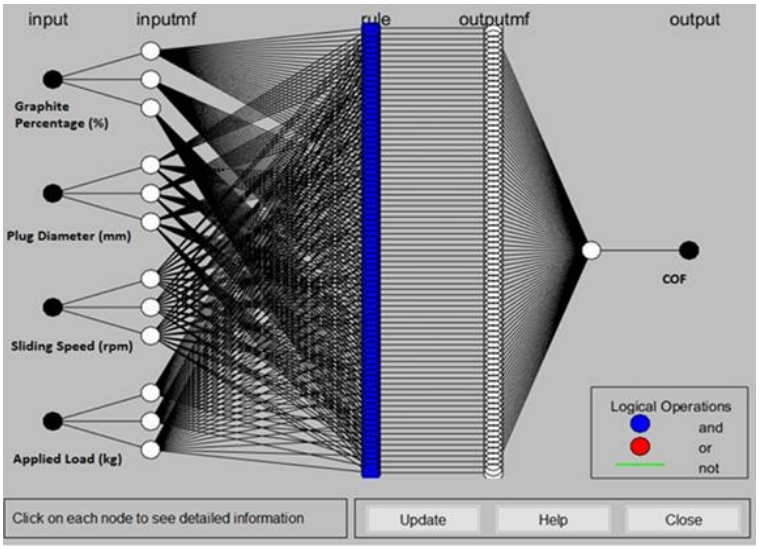


Figure 2. Generation of the ANFIS predictive model for coefficient of friction (COF)

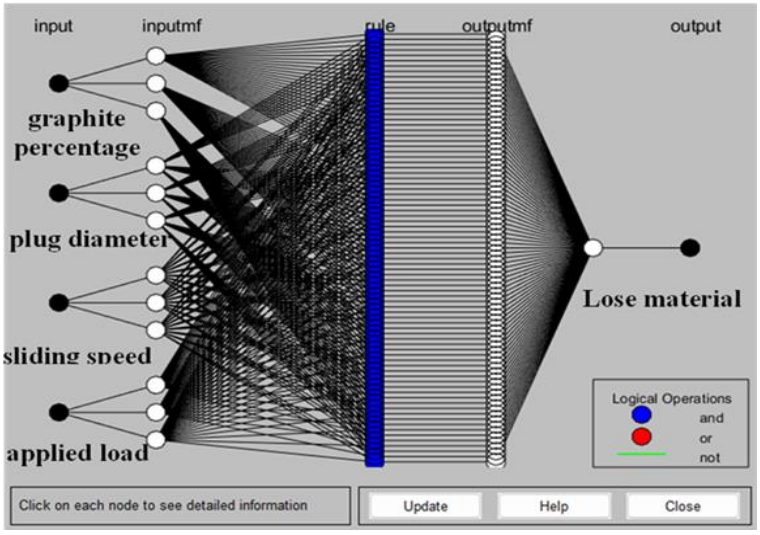


Figure 3. Generation of the ANFIS predictive model for material loss

Step 2a – Model Generalisation and the 81 Rules. The number of fuzzy rules is equal to the number of training conditions, but this does not mean that they are directly memorising the training data set. In the ANFIS models based on grid partitioning, the fuzzy "IF–THEN" rules are generated by partitioning the n-dimensional input space into subregions, which means that each rule represents a region of the input space instead of a single experimental point (Karaboga & Kaya, 2019; Rajab, 2019). Because the membership functions overlap, individual samples typically activate multiple rules simultaneously with different firing strengths (membership grades), and the consequent parameters of all rules are estimated from all activated samples, commonly using least-squares or hybrid gradient/least-squares algorithms (Jang, 1993; Karaboga & Kaya, 2019; Walia, 2015). The results from both the validation conditions (at parameter combinations not used in the training) showed errors lower than 4%, thus giving direct empirical evidence that the model generalises and does not memorise them. When used for validation under operating conditions not included in the training process, it is observed that these models are able to

accurately predict their outputs at the points that are not seen during the training process, and the resulting surfaces are smooth and physically consistent with the processes they represent (Rajab, 2019). The behaviours show that the ANFIS models had the ability to interpolate and generalise, not just recall experimental values.

Step 3 — Fuzzy logic design. The fuzzy inference used the product T-norm for rule-firing strength (Layer 2) and weighted average defuzzification (Layer 5). The zero-order TSK structure was chosen because it provides a set of 81 singleton consequent parameters (one for each rule, estimated by the least-squares method) and 36 premise parameters (four input parameters, 3 triangular membership functions, and 3 shape parameters for each, updated by the gradient descent optimization method), a total of 117 adjustable parameters per model. A comparison with a reduced 16-rule architecture was not performed, but rather the 81-rule structure directly follows from the application of the full-factorial 3×3×3×3 grid partitioning scheme to the four input variables.

Step 4 — Training. The hybrid learning algorithm was applied over 200 epochs. In the forward pass, consequent parameters were fit by least-squares estimation. The backward pass updated premise parameters through gradient-descent backpropagation. MATLAB ANFIS reports training convergence using root mean square error (RMSE) at each epoch (MathWorks Inc., 2024). RMSE is also widely employed in tribology-oriented artificial intelligence models for evaluating predictive accuracy and generalization capability (Jayasinghe & Ramezani, 2025). Importantly, across the literature on ANFIS and artificial neural networks, RMSE is used explicitly as a training error metric—it quantifies the difference between predicted and actual values during the learning phase and decreases with training epochs (Obianyo, Udeala, & Alaneme, 2023; Uthathip, Bhasaputra, & Pattaraprakorn, 2022). For example, (Obianyo et al., 2023) report training and testing RMSE separately for ANN and ANFIS models in construction scheduling, while (Uthathip et al., 2022) plot training RMSE against epoch number to monitor convergence in vehicle fuel-consumption prediction.

Both ANFIS models converged before the epoch limit, with final RMSE values of 0.00097889 for COF and 0.00636561 g for material loss. Prediction accuracy at each operating condition was calculated using the percentage error equation in equation (2), which divides the absolute difference between experimental and predicted values by the experimental value and converts the result to a percentage:

$$\text{Error} = \left|\frac{\text{Experimental}-\text{ANFIS}}{\text{Experimental}}\right| \times 100 \qquad (2)$$

The training convergence curves for COF and material loss are shown in Figures 5 and 7, and the corresponding training data versus FIS output plots are shown in Figures 6 and 8, confirming that the ANFIS training error had stabilized before the 200-epoch limit was reached. These figures show training convergence, not COF–time friction traces; the steady-state friction behavior was confirmed during the experiments by the plateauing of the COF–time curves recorded every 2 minutes throughout each test.

Step 5 — Fuzzy rule generation. Grid partitioning automatically generated 81 IF-THEN rules of the zero-order TSK form. Each rule takes the structure IF (graphite is A_i) AND (diameter is B_i) AND (speed is C_i) AND (load is D_i), THEN output = f_i, where f_i is a constant updated during training. The rule base governing input-output relationships for COF and material loss are shown in Figures 9 and 10.

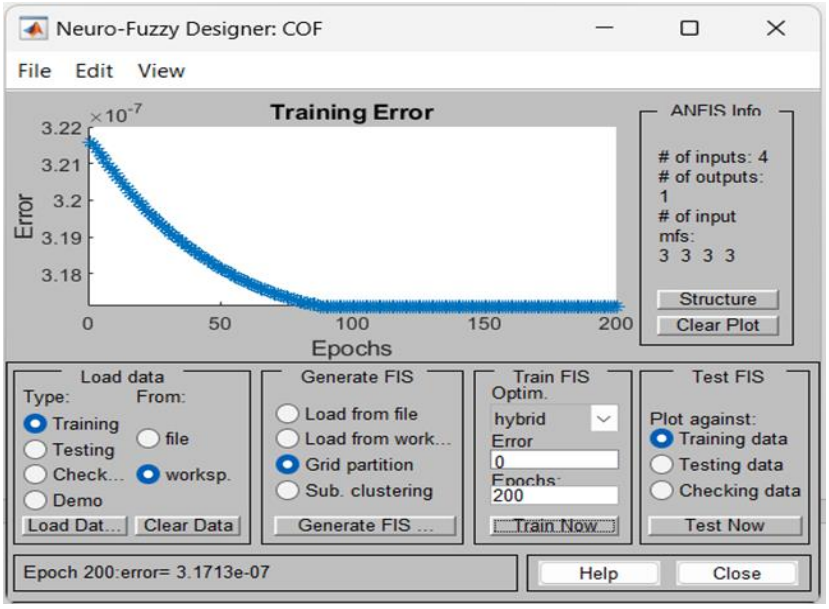


Figure 4. Training RMSE convergence of the ANFIS model for coefficient of friction (COF) prediction

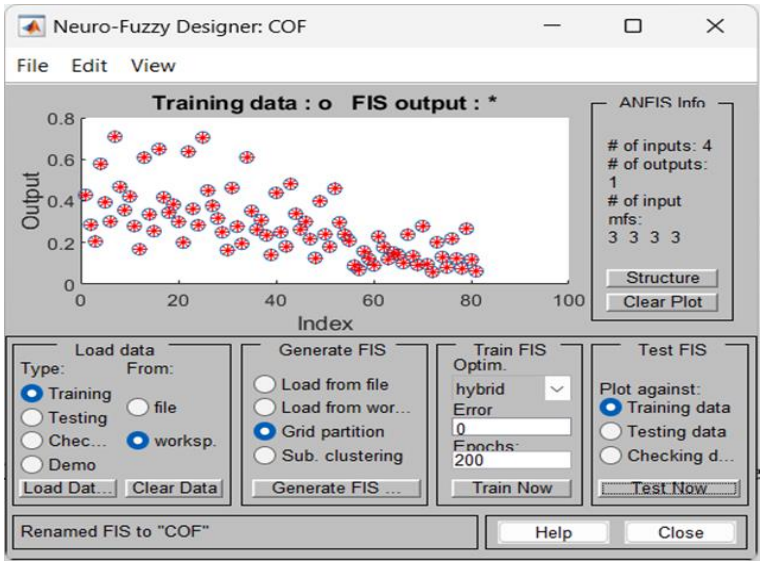


Figure 5. Training data vs. FIS output for the COF model across all 81 training conditions

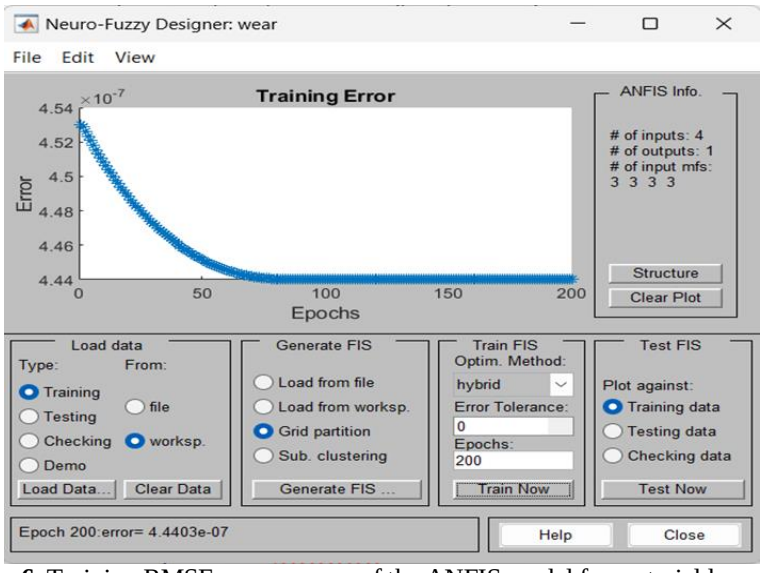


Figure 6. Training RMSE convergence of the ANFIS model for material loss prediction

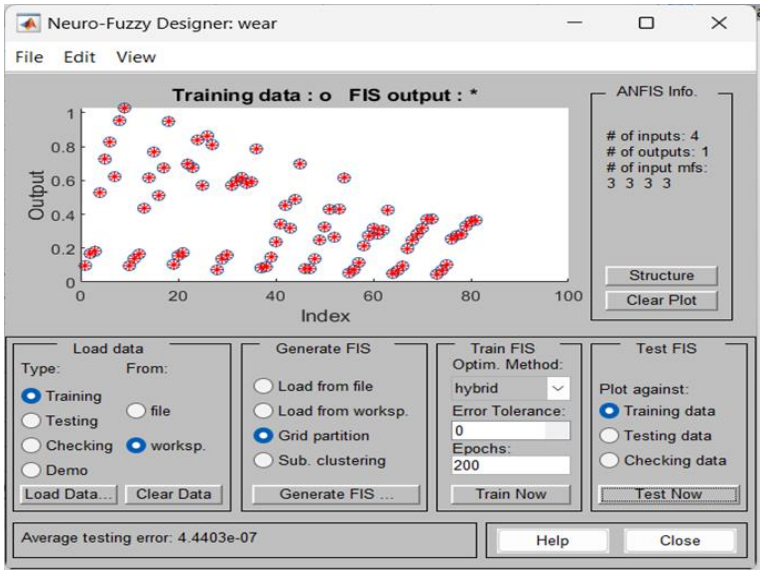


Figure 7. Training data vs. FIS output for the material loss model across all 81 training conditions

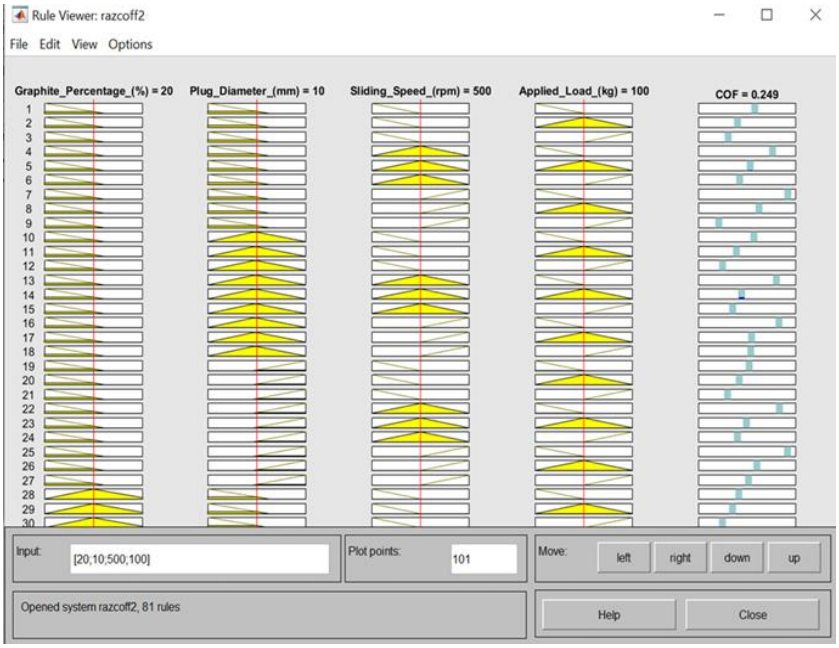


Figure 9. ANFIS rule viewer for the COF model

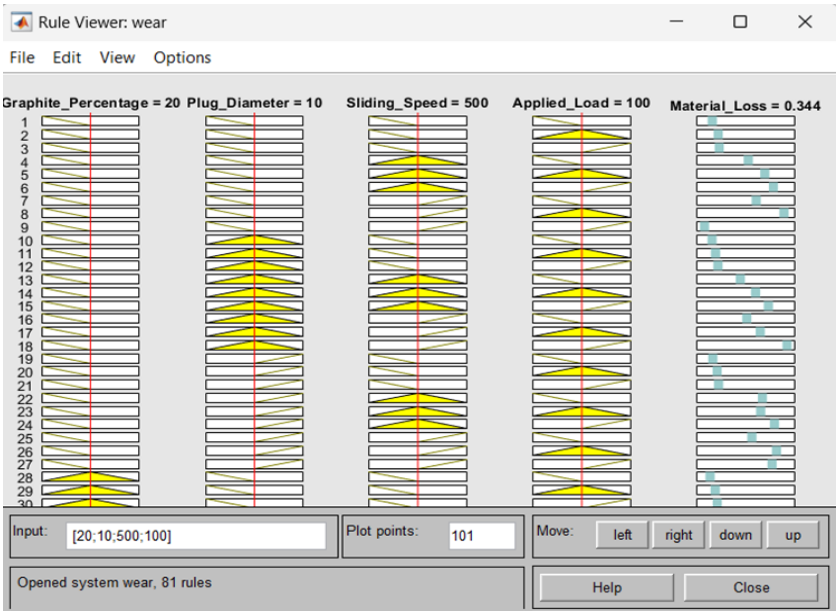


Figure 10. ANFIS rule viewer for the material loss model

Step 6 — Validation. Three additional experiments were conducted at operating conditions not included in the 81-point training set. The trained ANFIS model predicted the output at each validation condition, and the percentage error between predicted and experimental values was calculated using equation (2).

As discussed in Step 2a, although the number of fuzzy rules (81) equals the number of training conditions, this should not be interpreted as direct memorization of the dataset. In ANFIS models that use grid partitioning, the fuzzy "IF–THEN" rules are constructed by dividing the multidimensional input space into subregions; each rule therefore corresponds to a region of the input space rather than to a single experimental point (Babanezhad, Nakhjiri, & Shirazian, 2020; Karaboga & Kaya, 2019). Because the membership functions (e.g., triangular or sigmoidal-difference types) overlap, individual samples typically activate multiple rules simultaneously with different firing strengths (membership grades), and the consequent parameters of all rules are estimated from all activated samples, commonly using least-squares or hybrid gradient/least-squares algorithms (Jang, 1993; Karaboga & Kaya, 2019; Walia, 2015). Validation at operating conditions that were not used in training shows that these models can accurately predict outputs at unseen points, and the resulting surfaces are smooth and physically consistent with the underlying processes (Babanezhad et al., 2020). These behaviors indicate that the ANFIS models retained interpolation and generalization capability, rather than merely reproducing stored experimental values.

3. RESULTS AND DISCUSSION

4.1 ANFIS Model for Coefficient of Friction

After 200 training epochs, the COF model converged to a final training RMSE of 0.00097889, indicating highly stable convergence and accurate interpolation across the investigated operating conditions. This reflects the relatively smooth and monotonic response of the friction coefficient to the four input variables across the tested parameter space. The training predictions for COF are shown in Table 6.

In all configurations, the COF decreases as the applied load is increased. The 50 kg load produced the highest COF values, whereas the COF values at 150 kg were approximately 34–79% lower (mean reduction of about 55% across the 27 graphite/diameter/speed combinations), depending on the configuration. For instance, at a 10% graphite content, 8 mm plug diameter and 250 rpm, COF drops from about 0.429 at 50 kg to about 0.205 at 150 kg, which is a 52% reduction.

This inverse relationship between COF and normal load is in agreement with the fundamental Bowden and Tabor model of friction (Hsia, 2023). As normal load rises, the real contact area rises, but for the self-lubricating bronze/graphite systems, as the contact pressure rises, the graphite gets extruded and compacted to form a denser and more uniform lubricating layer with the basal planes oriented preferentially in the sliding direction, which lowers the interfacial shear strength. The inverse load-COF relationship is most significant in the range of 30% coverage of the graphite because enough graphite is present to provide a continuous lubricating film.

The 81 fuzzy rules suggest that increasing graphite coverage consistently decreases friction – consistent with the well-established solid lubrication mechanism of graphite. The influence of applied load and sliding speed on COF is more complicated: the response surfaces (Figure 11a–d) indicate that COF tends to rise with sliding speed, but tends to fall with increasing applied load. This inverse load-COF relationship is consistent with the mechanism of pressure-activated graphite extrusion and compaction discussed earlier. The 3D response surfaces (Figure 11a–d) show the combined influence of input pairs. The surface for graphite percentage versus plug diameter (Figure 11a) shows the strongest friction reduction at 30% graphite coverage regardless of plug diameter, confirming that surface coverage percentage dominates over plug geometry. The surface for sliding speed versus applied load (Figure 11c) shows COF rising with sliding speed but falling with applied load, consistent with the inverse load-COF relationship discussed above; the speed-driven increase reflects intensified asperity contact and frictional heat generation at higher sliding speeds, while the load-driven decrease reflects the pressure-activated graphite extrusion and compaction mechanism.

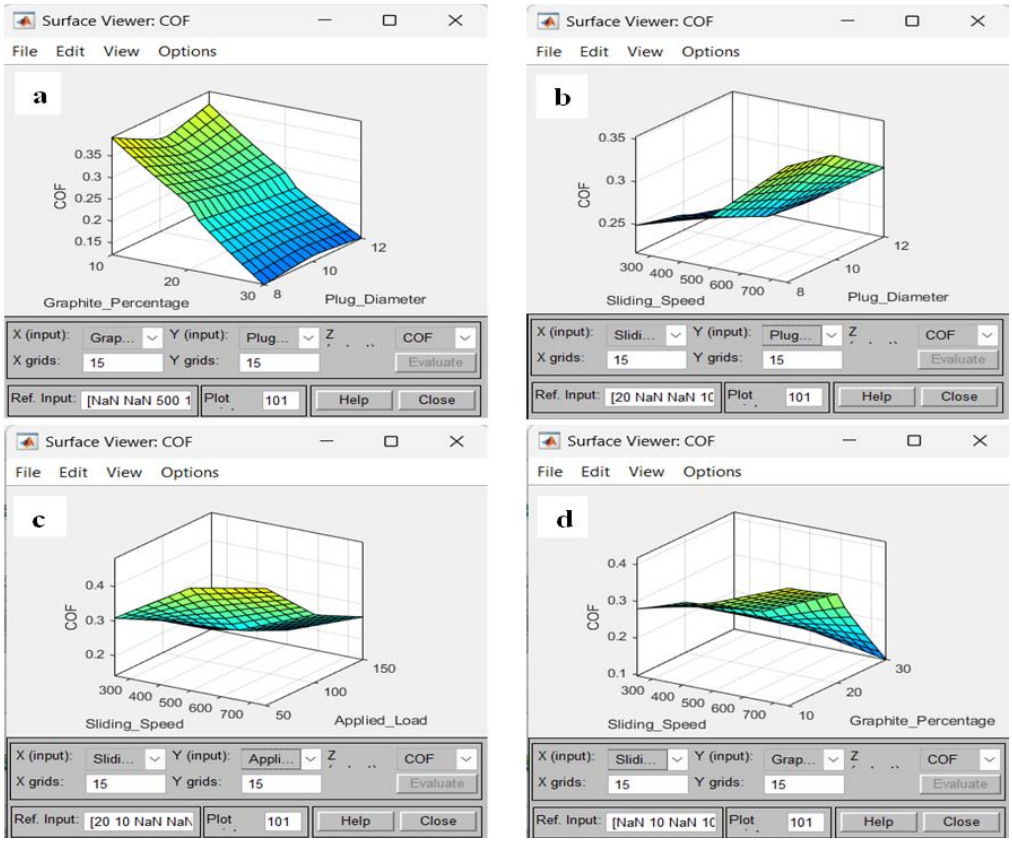


Figure 8. 3D response surfaces — COF: (a) graphite % vs. plug diameter; (b) speed vs. plug diameter; (c) speed vs. load; (d) speed vs. graphite %

Table 6. Coefficient of friction training predictions (ANFIS vs. experimental)

Graphite Percentage (%)	Plug Diameter (mm)	Sliding Speed (rpm)	Applied Load (kg)	Experimental COF	ANFIS COF	Absolute Error	Percentage Error (%)
10	8	250	50	0.429	0.428991344	8.65591E-06	0.002017694
10	8	250	100	0.286	0.285544805	0.000455195	0.159158977
10	8	250	150	0.204749937	0.204660013	8.99238E-05	0.043918824
10	8	500	50	0.5785	0.578492116	7.8841E-06	0.001362852
10	8	500	100	0.3926	0.392011613	0.000588387	0.149869307
10	8	500	150	0.301707405	0.30160977	9.76351E-05	0.032360848
10	8	750	50	0.7085	0.708499439	5.61013E-07	7.91832E-05
10	8	750	100	0.468	0.467244407	0.000755593	0.161451419
10	8	750	150	0.355874891	0.355758332	0.000116559	0.03275279
10	10	250	50	0.420875	0.42055793	0.00031707	0.075336019
10	10	250	100	0.2795	0.277269859	0.002230141	0.797903745
10	10	250	150	0.167916662	0.160103396	0.007813266	4.653061557
10	10	500	50	0.60775	0.612211752	0.004461752	0.734142593
10	10	500	100	0.336375	0.324400541	0.011974459	3.559854068
10	10	500	150	0.254583255	0.245025028	0.009558227	3.754460199
10	10	750	50	0.65	0.637629837	0.012370163	1.903101987
10	10	750	100	0.417625	0.406706348	0.010918652	2.614463106
10	10	750	150	0.34341561	0.340083992	0.003331618	0.970141639
10	12	250	50	0.381875	0.381860451	1.45489E-05	0.003809869
10	12	250	100	0.299	0.298735985	0.000264015	0.088299453
10	12	250	150	0.199333327	0.19922471	0.000108617	0.054490207
10	12	500	50	0.637	0.636995497	4.50254E-06	0.000706835
10	12	500	100	0.362375	0.361507261	0.000867739	0.239458884
10	12	500	150	0.282749991	0.28266216	8.78314E-05	0.031063266
10	12	750	50	0.70525	0.70524934	6.60309E-07	9.36276E-05
10	12	750	100	0.450125	0.449323438	0.000801562	0.178075495
10	12	750	150	0.375916655	0.37583966	7.69949E-05	0.020481916
20	8	250	50	0.31525	0.308691817	0.006558183	2.080311716
20	8	250	100	0.248625	0.246276073	0.002348927	0.944767106
20	8	250	150	0.164124495	0.16169549	0.002429005	1.479977036
20	8	500	50	0.463125	0.456472913	0.006652087	1.436348169
20	8	500	100	0.27625	0.268958998	0.007291002	2.639276609
20	8	500	150	0.193916661	0.187621082	0.006295579	3.246538504
20	8	750	50	0.609375	0.603666858	0.005708142	0.936720812
20	8	750	100	0.352625	0.345172258	0.007452742	2.113503719
20	8	750	150	0.26324919	0.257824503	0.005424687	2.060666018
20	10	250	50	0.30875	0.301359056	0.007390944	2.393827854
20	10	250	100	0.234	0.228998591	0.005001409	2.137354178
20	10	250	150	0.1408329	0.13556217	0.00527073	3.742541496
20	10	500	50	0.43875	0.425345908	0.013404092	3.055063692
20	10	500	100	0.2494375	0.239608426	0.009829074	3.940495911
20	10	500	150	0.18199944	0.176058564	0.005940876	3.26422757
20	10	750	50	0.481	0.447881085	0.033118915	6.885429332
20	10	750	100	0.338	0.332110804	0.005889196	1.742365537
20	10	750	150	0.263790855	0.260272602	0.003518253	1.333728141
20	12	250	50	0.299	0.294222767	0.004777233	1.597736677
20	12	250	100	0.216125	0.211091451	0.005033549	2.328998955
20	12	250	150	0.12674961	0.122474853	0.004274757	3.372599564
20	12	500	50	0.398125	0.384366836	0.013758164	3.455739782
20	12	500	100	0.2396875	0.232143232	0.007544268	3.147543437
20	12	500	150	0.17983278	0.173842682	0.005990098	3.330926893
20	12	750	50	0.45825	0.444027354	0.014222646	3.103687046
20	12	750	100	0.297375	0.288091265	0.009283735	3.121895026
20	12	750	150	0.23724927	0.229203184	0.008046086	3.391406095
30	8	250	50	0.209625	0.205818529	0.003806471	1.81584796

30	8	250	100	0.0885625	0.082101379	0.006461121	7.295549092
30	8	250	150	0.068791455	0.065196881	0.003594574	5.225320105
30	8	500	50	0.157625	0.146129451	0.011495549	7.292973347
30	8	500	100	0.121875	0.116099422	0.005775578	4.738936149
30	8	500	150	0.089374725	0.085559904	0.003814821	4.268344144
30	8	750	50	0.229125	0.214723078	0.014401922	6.285618014
30	8	750	100	0.177125	0.170493569	0.006631431	3.743927176
30	8	750	150	0.12133296	0.116024206	0.005308754	4.375359811
30	10	250	50	0.15275	0.134696921	0.018053079	11.81870996
30	10	250	100	0.143	0.150429518	0.007429518	5.195467455
30	10	250	150	0.101291355	0.106760398	0.005469043	5.399318424
30	10	500	50	0.23725	0.245697274	0.008447274	3.560495028
30	10	500	100	0.134875	0.133302934	0.001572066	1.165572907
30	10	500	150	0.092624715	0.090499643	0.002125072	2.294281731
30	10	750	50	0.2795	0.28299973	0.00349973	1.252139544
30	10	750	100	0.095875	0.069966297	0.025908703	27.02341861
30	10	750	150	0.05958315	0.040037787	0.019545363	32.8035066
30	12	250	50	0.2015	0.197933417	0.003566583	1.77001662
30	12	250	100	0.131625	0.128341868	0.003283132	2.494307517
30	12	250	150	0.08016642	0.078484175	0.001682245	2.098440732
30	12	500	50	0.219375	0.213027772	0.006347228	2.893323279
30	12	500	100	0.1235	0.119010023	0.004489977	3.635608635
30	12	500	150	0.076374765	0.072576991	0.003797774	4.972550272
30	12	750	50	0.2665	0.259673512	0.006826488	2.561533788
30	12	750	100	0.118625	0.111626416	0.006998584	5.899754481
30	12	750	150	0.06174981	0.055249734	0.006500076	10.52647048

4.2 Model Validation — Coefficient of Friction

To assess the generalization capability of the trained COF model, three experiments were conducted at operating conditions that were not part of the 81-point training set. These validation conditions were deliberately chosen at intermediate parameter values—between the training levels—to test the model's interpolation accuracy. The ANFIS model was used to predict COF at each condition, and the percentage error between the predicted and experimental values was calculated using equation (2). Results are presented in Table 7.

Table 7. COF validation results (three unseen operating conditions)

Graphite (%)	Plug Dia. (mm)	Speed (rpm)	Load (kg)	COF EXP.	COF ANFIS	Error (%)
10	8	350	70	0.419	0.424	1.2
20	10	400	125	0.202	0.203	0.2
30	12	670	140	0.0765	0.0768	0.39

The maximum validation error of 1.20% indicates satisfactory interpolation accuracy within the investigated parameter range (MathWorks Inc., 2024), confirming that the COF model generalizes reliably to interpolated operating conditions outside the training dataset.

The three validation experiments listed in Table 7 are experimental tests that were not used in the training set of 81 points but were performed specifically for this study. The target conditions for validation were intentionally selected at intermediate parameter values (e.g. 350 rpm, 400 rpm, 670 rpm; 70 kg, 125 kg, 140 kg) to assess the model's capability to predict performance at conditions other than those used in training.

Speed and load exhibit the most nonlinear tribological behavior in graphite-plugged bronze bushings (Alsammarraie et al., 2026). The most stringent test of the predictive power of the model is the ability to predict the interstitial behavior in these dimensions, since the frictional heating and wear mechanisms are most sensitive to these parameters. The percentage of graphite and plug diameter, however, are discrete design variables, where engineers usually choose from available standard options (10%, 20%, 30%; 8 mm, 10 mm, 12 mm).

The main use of the ANFIS model is to forecast the performance of the bushing under different loads and speeds for a particular bushing design. Thus, the model's applicability to engineering practice is most satisfactorily tested by its ability to be validated against intermediate loads and speeds.

The presented validation technique (three independent experiments) is similar to the standard practice for ANFIS modelling in tribological applications (Obianyo et al., 2023; Uthathip et al., 2022), where 2-5 validation points are usually employed to validate the model reliability. In

the future, extensions of this research may encompass a wider array of validation data sets, k-fold cross-validation, or leave-one-out cross-validation to further ensure a stronger reliability measure of the model. The present validation results (max. error 1.20% for COF), however, already offer strong evidence of the generalization ability of the model in the interpolated range.

Milčić et al. (2021) reported very low prediction deviations for COF in lubricated tin-babbitt bearings using ANN-based models with fewer input variables and simpler operating conditions. Despite the greater complexity of the present four-input dry-sliding system, the developed ANFIS model maintained comparably strong predictive performance.

4.3 ANFIS Model for Material loss

The material loss model reached a final RMSE of 0.00636561 g after 200 epochs. Predictions tracked measured values well across most conditions (Table 8).

However, four cases produced notable errors: a maximum error of 40.86% at 20% graphite, 10 mm diameter, 500 rpm, and 50 kg load; 23.59% at 20% graphite, 10 mm diameter, 750 rpm, and 50 kg load; 22.22% at 20% graphite, 10 mm diameter, 500 rpm, and 100 kg load; and 14.42% at 20% graphite, 10 mm diameter, 250 rpm, and 100 kg load.

The 20% graphite, 10 mm plug configuration always generated the highest training error. This is the most sensitive configuration in the parameter space, where the tribological regime is in between the lubricant-starved and partially lubricated regimes. The non-monotonic response to wear in this region (increasing wear as the graphite content increases from 10% to 20% to 30%) is beyond the interpolation capacity of a uniform three-level grid partition using triangular membership functions. Non-monotonic behavior occurs in these errors, which occur in transition zones and cannot be resolved completely by a uniform 3-level grid partition. Future work may focus on this development by employing a non-uniform grid or an adaptive subtractive clustering method to create higher resolution in this transition zone.

The broader wear trends across the operating space still emerged clearly. The 3D response surfaces (Figure 12a–d) indicate that material loss increases with both sliding speed and applied load, as expected for dry-sliding metallic contacts where frictional energy dissipation governs material removal. Higher graphite content and larger plug diameter reduce wear in most of the tested configurations (24 of the 27 diameter/speed/load combinations show a monotonic decrease in wear from 10% to 30% graphite), consistent with the transfer film formation mechanism; the exceptions all occur at the 10 mm plug diameter. The non-monotonic wear behavior at 20% graphite coverage is consistent with findings by (Stojanović, Babić, Veličković, & Blagojević, 2016) for aluminum hybrid composites with graphite, where intermediate graphite concentrations produce competing abrasion and lubrication effects that resist monotonic trend prediction.

Table 8. Material loss training predictions (ANFIS vs. experimental)

Graphite Percentage (%)	Plug Diameter (mm)	Sliding Speed (rpm)	Applied Load (kg)	Experimental Wear (g)	ANFIS Wear (g)	Absolute Error	Percentage Error (%)
10	8	250	50	0.0977	0.097640148	5.98524E-05	0.061261375
10	8	250	100	0.1685	0.168471577	2.84228E-05	0.016868154
10	8	250	150	0.1812	0.181177727	2.22728E-05	0.012291812
10	8	500	50	0.5279	0.527770844	0.000129156	0.02446599
10	8	500	100	0.725	0.724917042	8.29581E-05	0.011442501
10	8	500	150	0.8272	0.827192159	7.8408E-06	0.000947873
10	8	750	50	0.6222	0.621989528	0.000210472	0.03382712
10	8	750	100	0.9523	0.952244242	5.57579E-05	0.005855079
10	8	750	150	1.028	1.027999239	7.61197E-07	7.40464E-05
10	10	250	50	0.0955	0.094377622	0.001122378	1.175265173
10	10	250	100	0.1372	0.127864099	0.009335901	6.80459229
10	10	250	150	0.1653	0.160622034	0.004677966	2.829985199
10	10	500	50	0.4355	0.396425355	0.039074645	8.972363911
10	10	500	100	0.615	0.582571926	0.032428074	5.272857502
10	10	500	150	0.7682	0.748698944	0.019501056	2.538538951
10	10	750	50	0.5108	0.478054539	0.032745461	6.410622733
10	10	750	100	0.6731	0.588718366	0.084381634	12.53627012
10	10	750	150	0.9471	0.933487474	0.013612526	1.437284971
10	12	250	50	0.1046	0.104546812	5.31884E-05	0.050849298
10	12	250	100	0.1562	0.156169286	3.07139E-05	0.019663169
10	12	250	150	0.1738	0.173777043	2.29565E-05	0.01320859
10	12	500	50	0.696	0.696017083	1.7083E-05	0.002454459
10	12	500	100	0.6753	0.675173685	0.000126315	0.018705074

10	12	500	150	0.839	0.839000218	2.17949E-07	2.59772E-05
10	12	750	50	0.5711	0.57091308	0.00018692	0.03272988
10	12	750	100	0.864	0.864037528	3.75277E-05	0.004343483
10	12	750	150	0.8112	0.811199262	7.38377E-07	9.10228E-05
20	8	250	50	0.0717	0.070737602	0.000962398	1.342256092
20	8	250	100	0.1346	0.133386331	0.001213669	0.90168587
20	8	250	150	0.1582	0.157383486	0.000816514	0.516127593
20	8	500	50	0.5711	0.572590498	0.001490498	0.260987169
20	8	500	100	0.5973	0.592840491	0.004459509	0.74661121
20	8	500	150	0.618	0.610709159	0.007290841	1.179747686
20	8	750	50	0.582	0.580600725	0.001399275	0.240425175
20	8	750	100	0.5917	0.578999386	0.012700614	2.146461673
20	8	750	150	0.786	0.777572979	0.008427021	1.07214012
20	10	250	50	0.0826	0.085337446	0.002737446	3.314099128
20	10	250	100	0.0897	0.076767338	0.012932662	14.41768367
20	10	250	150	0.1462	0.14294298	0.00325702	2.227783593
20	10	500	50	0.2374	0.140396163	0.097003837	40.86092555
20	10	500	100	0.3436	0.267255537	0.076344463	22.21899386
20	10	500	150	0.4512	0.39675741	0.05444259	12.06617692
20	10	750	50	0.317	0.242235097	0.074764903	23.58514289
20	10	750	100	0.4879	0.459258441	0.028641559	5.870374946
20	10	750	150	0.6973	0.669803628	0.027496372	3.943262809
20	12	250	50	0.0795	0.078622639	0.000877361	1.10359828
20	12	250	100	0.0783	0.075535439	0.002764561	3.5307295
20	12	250	150	0.1373	0.136019394	0.001280606	0.932706255
20	12	500	50	0.248	0.232348604	0.015651396	6.311046656
20	12	500	100	0.325	0.312724543	0.012275457	3.777063599
20	12	500	150	0.429	0.414716537	0.014283463	3.329478596
20	12	750	50	0.2645	0.253720352	0.010779648	4.075481249
20	12	750	100	0.4319	0.41671576	0.01518424	3.515684164
20	12	750	150	0.614	0.607132943	0.006867057	1.118413203
30	8	250	50	0.0531	0.052783199	0.000316801	0.596611681
30	8	250	100	0.0725	0.07143012	0.00106988	1.475696892
30	8	250	150	0.1157	0.114987139	0.000712861	0.616128737
30	8	500	50	0.2137	0.207581795	0.006118205	2.862987836
30	8	500	100	0.274	0.268568725	0.005431275	1.982217183
30	8	500	150	0.3166	0.31161607	0.00498393	1.574203969
30	8	750	50	0.2816	0.276521924	0.005078076	1.803294119
30	8	750	100	0.3054	0.300679014	0.004720986	1.545837088
30	8	750	150	0.425	0.419030068	0.005969932	1.404689773
30	10	250	50	0.0497	0.048399901	0.001300099	2.615892567
30	10	250	100	0.0686	0.067351581	0.001248419	1.819853473
30	10	250	150	0.0944	0.087385959	0.007014041	7.430128353
30	10	500	50	0.1982	0.191863244	0.006336756	3.197152439
30	10	500	100	0.246	0.236495879	0.009504121	3.863463691
30	10	500	150	0.284	0.27343126	0.01056874	3.721387484
30	10	750	50	0.3157	0.325140205	0.009440205	2.990245435
30	10	750	100	0.37	0.38651914	0.01651914	4.464632461
30	10	750	150	0.3732	0.354859177	0.018340823	4.914475741
30	12	250	50	0.0457	0.045119976	0.000580024	1.269198478
30	12	250	100	0.06941	0.069274268	0.000135732	0.19555165
30	12	250	150	0.103	0.102434558	0.000565442	0.548972885
30	12	500	50	0.253	0.253332711	0.000332711	0.131506232
30	12	500	100	0.2744	0.273741463	0.000658537	0.239991654
30	12	500	150	0.283	0.2807666	0.0022334	0.789187256
30	12	750	50	0.331	0.332291317	0.001291317	0.390126025
30	12	750	100	0.357	0.355983406	0.001016594	0.284760136
30	12	750	150	0.364	0.35988304	0.00411696	1.13103307

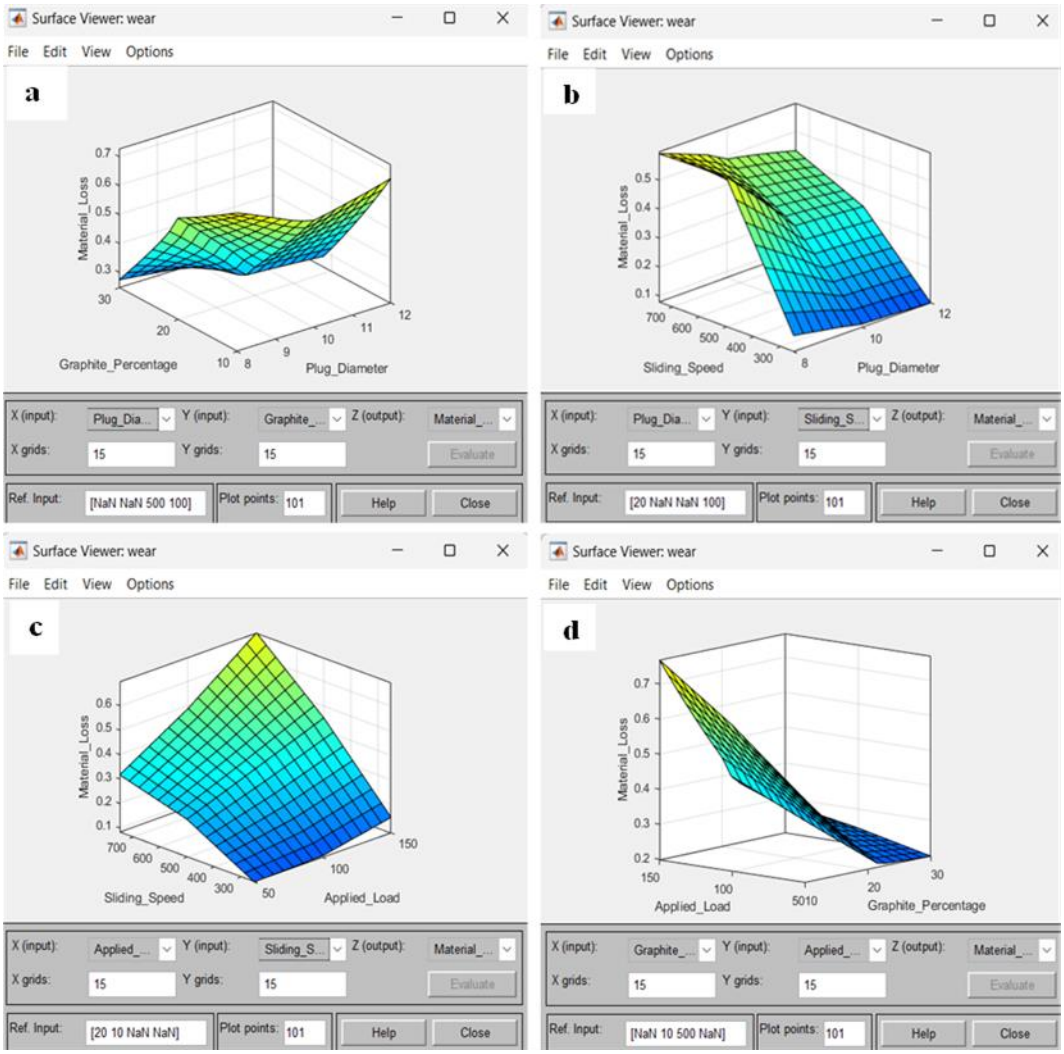


Figure 9. 3D ANFIS response surfaces for material loss: (a) graphite % vs. plug diameter; (b) sliding speed vs. plug diameter; (c) sliding speed vs. applied load; (d) sliding speed vs. graphite %

4.4 Model Validation — Material loss

To assess the generalization capability of the material loss model, three validation experiments were performed at the same intermediate operating conditions used for COF validation. The ANFIS model predicted material loss at each condition, and percentage errors were calculated using equation (2). Table 9 presents the results.

The maximum validation error of 3.927% indicates satisfactory interpolation accuracy for material loss prediction within the investigated parameter range (MathWorks Inc., 2024). The larger error compared to the COF model is attributed to the sensitivity of material loss to operating conditions under dry sliding, particularly around intermediate graphite contents, where adhesive and abrasive wear mechanisms overlap and the response becomes harder to predict. However, the three validation results (Table 9: 0.331 g at 10% graphite, 0.285 g at 20% graphite, 0.337 g at 30% graphite) do not show a consistent drop in material loss as graphite content increases; material loss is lowest at the intermediate 20% graphite condition and highest at 30%. Moreover, because each of the three validation cases simultaneously changes graphite content, plug diameter, sliding speed, and applied load, these three points cannot be used in isolation to infer a graphite-content effect on material loss; any such effect can only be assessed from the controlled 81-point factorial training data (Table 8), where graphite content is varied while other factors are held at fixed levels.

Table 9. Material loss validation results (three unseen operating conditions)

Graphite (%)	Plug Dia. (mm)	Speed (rpm)	Load (kg)	WL Exp (g)	WL ANFIS	Error (%)
10	8	350	70	0.331	0.318	3.927
20	10	400	125	0.2850	0.286	0.351
30	12	670	140	0.3250	0.337	3.692

4.5 Comparative Model Performance

Table 10 consolidates the main performance metrics for both models. This use of RMSE as a training-error metric follows standard practice in ANFIS modelling (Obianyo et al., 2023; Uthathip et al., 2022). The material loss model came in at 0.00636561 g RMSE and 3.927% maximum error—wear behavior under dry sliding is more nonlinear, so the larger spread is expected. Both figures indicate satisfactory interpolation accuracy within the investigated parameter range. Using RMSE as the primary metric is consistent with recent AI-based tribology work on ANN and RNN models (Jayasinghe & Ramezani, 2025).

A more comprehensive evaluation of model performance is presented in Table 11, which reports additional metrics including training and validation MAE, MAPE, and R^2 values. These metrics were recalculated from the tabulated experimental and predicted values presented in Tables 6 and 8 using standard definitions.

Table 10. Consolidated ANFIS model performance summary

Output Variable	Final Training RMSE (MATLAB convergence output)	Maximum Validation Error (%)
Coefficient of Friction	0.00097889	1.20
Material loss (g)	0.00636561	3.927

Table 11. Comprehensive model performance metrics

Metric	COF Model	Material Loss Model
Training RMSE (MATLAB convergence output)	0.00097889	0.00636561 g
Training RMSE (calculated from Table 6/8 data)	0.008243	0.022087 g
Validation RMSE (from Table 7/9 data)	0.002949	0.010231 g
Training MAE	0.005884	0.010616 g
Validation MAE	0.002100	0.008667 g
Training MAPE	3.27%	3.29%
Validation MAPE	0.69%	2.66%
R^2 (Training)	0.9973	0.9928
R^2 (Validation)	0.9996	0.749

Two versions of the training RMSE are reported in Table 11: the value output by MATLAB during the hybrid-learning convergence process (0.00097889 for COF, 0.00636561 g for material loss), and the RMSE calculated directly from the experimental and ANFIS-predicted values tabulated in Tables 6 and 8 (0.008243 for COF, 0.022087 g for material loss). The two do not coincide; this discrepancy is attributed to MATLAB's ANFIS training algorithm operating on internally scaled/normalized variables during the hybrid learning process, whereas the values calculated here are RMSE on the raw, unscaled experimental and predicted quantities. All other metrics in Table 11 (MAE, MAPE, R^2, and validation RMSE) were calculated directly from the tabulated Tables 6-9 data to ensure internal consistency with the values presented elsewhere in the manuscript. On this consistent basis, the COF model generalizes well: validation MAE, MAPE, and R^2 are close to or better than the corresponding training values. The material loss model shows good agreement between training and validation MAE/MAPE, but the validation R^2 (0.749) is markedly lower than the training R^2 (0.9928). This reflects the small validation sample (n = 3), for which R^2 is highly sensitive to the specific points selected and should not be interpreted as evidence of poor generalization; the MAE, MAPE, and maximum percentage error provide a more reliable picture of validation performance for such a small validation set.

The maximum validation errors of 1.20% (COF) and 3.927% (material loss) indicate satisfactory interpolation accuracy within the investigated parameter range. These errors are comparable to or better than those reported in similar machine learning applications in tribology and materials engineering (Karaboga & Kaya, 2019). For reference, Sada and Ikpeseni (Sada & Ikpeseni, 2021) reported ANN and ANFIS prediction errors of a similar order of magnitude for AISI 1050 steel machining performance. The maximum validation errors obtained in the present study (1.20% for COF and 3.927% for material loss) are broadly consistent with the range of errors reported in that work; however, a numerical acceptance threshold derived from a different material system and process is not directly transferable to the present bushings and is not applied here as a pass/fail criterion.

The expanded uncertainties for the measurement systems, determined by GUM uncertainty propagation (Section 2.4), are as follows: normal force (±0.11 kg), friction force (±0.0202 kg), temperature (±3.9°C), mass loss (±0.054 mg), and surface roughness (±0.058 µm). These values quantify the uncertainty of the individual measured quantities (force, temperature, mass, and roughness) and cannot be compared directly to the ANFIS prediction errors for COF and material loss, since COF and material loss are each derived quantities computed from several measured inputs and the uncertainty of a derived quantity must be obtained through proper uncertainty propagation before any such comparison is made. For material loss specifically, the mass-loss measurement uncertainty (±0.054 mg) is far smaller than the absolute validation errors observed for the material loss model, which range from about 1 mg to 13 mg across the training and

validation datasets (Tables 8 and 9). The ANFIS prediction error for material loss is therefore not bounded by, nor comparable to, the mass-loss measurement uncertainty; it instead reflects the model's ability to capture the underlying nonlinear tribological response, which is a separate question from the precision of the balance used to weigh the bushings. A rigorous comparison between prediction error and experimental uncertainty for COF and material loss would require propagating the individual measurement uncertainties (force, geometry) through Equation (1) to obtain the uncertainty of COF itself and an equivalent propagation for material loss; this analysis has not been performed here, and the claim that prediction errors are within or near experimental uncertainty is accordingly withdrawn.

Both models held up well across the tested conditions. The COF model finished with a training RMSE of 0.00097889 and a maximum validation error of 1.20%; the material loss model came in at 0.00636561 g RMSE and 3.927%. The gap between them reflects the physics: COF responds fairly predictably to graphite content, while material loss behavior becomes more complex around 20% graphite, where abrasive and adhesive wear mechanisms overlap (Güngör & Demirer, 2022; MathWorks Inc., 2024). Training and validation errors stayed close, which suggests the models generalized rather than overfitting. Against Milčić et al. (2021), the present framework matched COF prediction accuracy using 81 experimental conditions across four input variables and added validated material loss predictions on top. The 81-rule IF–THEN structure also means the model's reasoning is readable—something black-box ANN models don't offer (Jang, 1993; Rajab, 2019; Walia, 2015).

4. CONCLUSIONS

This study covered the design and manufacture of a custom journal-bearing tribometer, a full factorial dry sliding experimental program on CuAl10Fe5Ni5 graphite-plugged bronze bushings running against an AISI 410 stainless steel shaft, and the development of two ANFIS models. The following conclusions are drawn:

1. Two independent ANFIS models were built for COF and material loss. Each uses a zero-order TSK fuzzy inference structure, a 3×3×3×3 grid partition, 81 IF-THEN rules, triangular membership functions, and 200 training epochs with a hybrid least-squares/gradient-descent algorithm (Jang, 1993).

2. MATLAB ANFIS training converged to final RMSE values of 0.00097889 for COF and 0.00636561 g for material loss. Validation against three previously unseen operating conditions gave maximum errors of 1.20% and 3.927% for COF and material loss, respectively—indicating satisfactory interpolation accuracy within the investigated parameter range—confirming reliable generalization to interpolated conditions.

3. The 3D response surfaces show physically consistent behavior: increasing graphite content and larger plug diameter reduce friction, while higher sliding speed and applied load drive up material loss. These trends are consistent with established solid lubrication theory and published data on bronze-graphite tribosystems (Cui, Bi, Yang, & Liu, 2014; Güngör & Demirer, 2022; Valente, Boutin, Rocha, do Vale, & da Silva, 2020).

4. The 81-rule IF-THEN structure provides physical interpretability unavailable from pure ANN models while maintaining prediction errors within 3.927%. The models can help reduce the extent of experimental testing required during the preliminary design of graphite-plugged bronze bushings (Jang, 1993; Rajab, 2019; Walia, 2015).

5. The demonstrated predictive capability applies primarily to interpolation within the investigated range of material and operating parameters (10-30% graphite, 8-12 mm plug diameter, 250-750 rpm, 50-150 kg load). Extrapolation beyond these ranges would require additional validation.

6. Three previously unseen conditions were used for validation – producing maximum errors of 1.20% (COF) and 3.927% (material loss), indicating satisfactory interpolation accuracy. Three validation conditions constitute a limited validation dataset.

Acknowledgement: The authors would like to thank Tikrit University for providing the laboratory facilities and technical support for this research.

References

Alambeigi, F., Khadem, S. M., Khorsand, H., & Mirza Seied Hasan, E. (2016). A comparison of performance of artificial intelligence methods in prediction of dry sliding wear behavior. *International Journal of Advanced Manufacturing Technology*, *84*(9–12), 1981–1994. https://doi.org/10.1007/s00170-015-7812-9

Alsammarraie, A., Zaidan, M. H., & Aljboury, A. K. A. (2026). A factorial analysis of material composition and operating parameters on tribological properties in graphite-plugged bronze bushings. *Research on Engineering Structures and Materials*, (in press). http://dx.doi.org/10.17515/resm2026-1428ma1222rs.

Babanezhad, M., Nakhjiri, A. T., & Shirazian, S. (2020). Changes in the Number of Membership Functions for Predicting the Gas Volume Fraction in Two-Phase Flow Using Grid Partition Clustering of the ANFIS Method. *ACS Omega*, *5*(26), 16284–16291. https://doi.org/10.1021/acsomega.0c02117

Cui, G., Bi, Q., Yang, J., & Liu, W. (2014). Effect of Normal Loads on Tribological Properties of Bronze-Graphite Composite under Seawater Condition. *Tribology Transactions*, *57*(2), 308–316. https://doi.org/10.1080/10402004.2013.877177

Güngör, K., & Demirer, A. (2022). Investigation of Dry Sliding Friction Wear Behavior of CuSn11 Bronze Plain Bearing Applying Impregnated Graphite-Filled PTFE. *Tribology Transactions*, *65*(5), 880–891. https://doi.org/10.1080/10402004.2022.2099496

Hsia, F.-C. (2023). *Nanoscale topography and wear of ceramic interfaces and their effect on macroscale friction* (Doctoral dissertation, University of Amsterdam, Enschede, Netherlands). Retrieved from https://dare.uva.nl

Jang, J.-S. R. (1993). ANFIS: adaptive-network-based fuzzy inference system. *IEEE Transactions on Systems, Man, and Cybernetics*, *23*(3), 665–685. https://doi.org/10.1109/21.256541

Jayasinghe, R., & Ramezani, M. (2025). AI-powered prediction of friction and wear in functionalized Epoxy-MWCNT composites. *Wear*, *582–583*(April), 206333. https://doi.org/10.1016/j.wear.2025.206333

Karaboga, D., & Kaya, E. (2019). Adaptive network based fuzzy inference system (ANFIS) training approaches: a comprehensive survey. *Artificial Intelligence Review*, *52*(4), 2263–2293. https://doi.org/10.1007/s10462-017-9610-2

Kumbhar, R., Gadade, A. M., Singh, R., & Choudhary, M. (2026). Tribo-Informatics Method for Predictive Modeling of Friction and Wear Mechanisms in Al7075/B4C Metal Matrix Composites. *Journal of Materials Engineering and Performance*. https://doi.org/10.1007/s11665-026-13723-3

Marhoon, S. G., & Al-Sammarraie, A. M. (2025). Based-predicting of tribological properties in brass and bronze under variable loads. *International Journal of Mechanical and Thermal Engineering*, *6*(2), 30–38. https://doi.org/10.22271/27078043.2025.v6.i2a.93

MathWorks Inc. (2024). anfis — Tune Sugeno-type fuzzy inference system using training data. Retrieved 15 May 2026, from MathWorks Documentation website: https://www.mathworks.com/help/fuzzy/anfis.html

Milčić, D., Alsammarraie, A., Madić, M., Krstić, V., & Milčić, M. (2021). Predictions of friction coefficient in hydrodynamic journal bearing using artificial neural networks. *Strojniski Vestnik/Journal of Mechanical Engineering*, *67*(9), 411–420. https://doi.org/10.5545/sv-jme.2021.7230

Ning, H., Chen, F., Su, Y., Li, H., Fan, H., Song, J., … Hu, L. (2024). Modeling and prediction of tribological properties of copper/aluminum-graphite self-lubricating composites using machine learning algorithms. *Friction*, *12*(6), 1322–1340. https://doi.org/10.1007/s40544-023-0847-2

Obianyo, J. I., Udeala, R. C., & Alaneme, G. U. (2023). Application of neural networks and neuro-fuzzy models in construction scheduling. *Scientific Reports*, *13*(1), 1–23. https://doi.org/10.1038/s41598-023-35445-5

Rajab, S. (2019). Handling interpretability issues in ANFIS using rule base simplification and constrained learning. *Fuzzy Sets and Systems*, *368*, 36–58. https://doi.org/10.1016/j.fss.2018.11.010

Sada, S. O., & Ikpeseni, S. C. (2021). Evaluation of ANN and ANFIS modeling ability in the prediction of AISI 1050 steel machining performance. *Heliyon*, *7*(2), e06136. https://doi.org/10.1016/j.heliyon.2021.e06136

Salim, M., Saini, D. S., Matharu, S. P. S., & Singh, M. (2023). Optimisation of Predicted Wear and Friction for Electroless Ni–P by RSM, Fuzzy Logic and ANFIS Using TOPSIS. *Transactions of the Indian Institute of Metals*, *76*(9), 2535–2548. https://doi.org/10.1007/s12666-023-02990-6

Stojanović, B., Babić, M., Veličković, S., & Blagojević, J. (2016). Tribological Behavior of Aluminum Hybrid Composites Studied by Application of Factorial Techniques. *Tribology Transactions*, *59*(3), 522–529. https://doi.org/10.1080/10402004.2015.1091535

Talpur, N., Salleh, M. N. M., & Hussain, K. (2017). An investigation of membership functions on performance of ANFIS for solving classification problems. *IOP Conference Series: Materials Science and Engineering*, *226*(1). https://doi.org/10.1088/1757-899X/226/1/012103

Ünlü, B. S., Durmuş, H., & Meriç, C. (2012). Determination of tribological properties at CuSn10 alloy journal bearings by experimental and means of artificial neural networks method. *Industrial Lubrication and Tribology*, *64*(5), 258–264. https://doi.org/10.1108/00368791211249647

Uthathip, N., Bhasaputra, P., & Pattaraprakorn, W. (2022). Application of ANFIS Model for Thailand's Electric Vehicle Consumption. *Computer Systems Science and Engineering*, *42*(1), 69–86. https://doi.org/10.32604/CSSE.2022.020120

Valente, C. A. G. S., Boutin, F. F., Rocha, L. P. C., do Vale, J. L., & da Silva, C. H. (2020). Effect of Graphite and Bronze Fillers on PTFE Tribological Behavior: A Commercial Materials Evaluation. *Tribology Transactions*, *63*(2), 356–370. https://doi.org/10.1080/10402004.2019.1695032

Vesović, M., & Jovanović, R. (2022). Adaptive neuro fuzzy Inference systems in identification, modeling and control: The state-of-the-art. *Tehnika*, *77*(5), 439–446. https://doi.org/10.5937/tehnika2204439v

Walia, N. (2015). *ANFIS: Adaptive Neuro-Fuzzy Inference System- A Survey*. *International Journal of Computer Applications, 123(13), 32–38*. https://doi.org/10.5120/ijca2015905635.

Zhu, L., Yi, M., Ge, Y., Zhang, B., & Xie, A. (2022). Intuitive Analysis of the Microtribological Behavior of Copper-Coated Graphite-Graphite/Cu Composites with High Graphite Contents. *ACS Omega*, *7*(32), 28217–28225. https://doi.org/10.1021/acsomega.2c01276

Ali K. A. Aljboury
Mechanical Department/ Engineering College/Tikrit University,
Tikrit,
Iraq
eng.alikhalaf1982@gmail.com
ORCID 0009-0004-3100-3439

Amir Alsammarraie
Mechanical Department/ Engineering College/Tikrit University,
Tikrit,
Iraq
amircraft@tu.edu.iq
ORCID 0000-0001-7934-1454

Maki H. Zaidan
Mechanical Department/ Engineering College/Tikrit University,
Tikrit,
Iraq
makihajzaidan@tu.edu.iq
ORCID 0000-0002-6067-4950